ORIGINAL ARTICLE

Eur. J. Anat. 24 (5): 399-406(2020)

The microanatomy of Bowman's layer in the cornea of the pig: Changes in collagen fibril architecture at the corneoscleral limbus

Greg M. Hammond[1], Robert D. Young[1], Duncan D. Muir[2], Andrew J. Quantock[1]

[1]Structural Biophysics Group, School of Optometry & Vision Sciences, Cardiff University, Maindy Road, Cathays, Cardiff, CF24 4HQ, Wales, UK, [2]School of Earth and Ocean Sciences, Cardiff University, Main Building, Park Place, Cardiff, CF10 3AT, Wales, UK

SUMMARY

In most animals, Bowman's layer is a feature of the cornea of the eye, and lies between the surface epithelium and the stromal extracellular matrix that makes up the bulk of the cornea. It is comprised of a condensation of disorganised collagen fibrils. However, it has been conjectured that not all species possess Bowman's layer, and pigs are a species that has classically been stated to lack this anatomical structure, although there is disagreement in the published literature. Here, we studied the porcine cornea using transmission and scanning electron microscopy (TEM and SEM) to ascertain whether Bowman's layer existed. TEM identified a thin band of disorganised collagen fibrils between the epithelial basement membrane and corneal stroma. SEM images of the central and peripheral corneal surfaces, following removal of the corneal epithelium by cell maceration, revealed a disorganised meshwork of collagen fibrils, with a highly aligned annulus of collagen at the limbus. In between the peripheral cornea and limbus, a "transition zone" is observed where collagen fibrils start to align. Quantification of fibril alignment demonstrates a significant increase in collagen alignment from 0.08 ± 0.04 to 0.33 ± 0.07 ($p < 0.001$; $n = 60$; 0 = no alignment, 1 = full alignment) with increasing distance from the corneal centre. These data together lead us to conclude that the porcine cornea does include Bowman's layer, though it is thin (contributing roughly 0.2% of corneal thickness), and thus, reaffirms the porcine cornea's similarity to its human counterpart and usefulness as a model system.

Key words: Bowman membrane – Cornea – Scanning electron microscopy – Transmission electron microscopy – Collagen – Porcine

INTRODUCTION

In most mammals, the cornea of the eye is comprised of four or five layers (Fig. 1). Distally, is the surface epithelium, a cellular multi-layer that supports the tear film and which is constantly replenished throughout life. Beneath these cells and their basement membrane lies Bowman's layer, a relatively thin acellular meshwork of collagen fibrils that is continuous with the anterior aspect of the corneal stroma. The collagen-rich corneal stroma, which is approximately 500 µm thick in the human cornea, represents the bulk of the tissue. Proximal to this is Descemet's membrane (the basement membrane of the corneal endothelium), and the

Corresponding author: Professor Andrew J Quantock. Structural Biophysics Group, School of Optometry & Vision Sciences, Cardiff University, Maindy Road, Cathays, Cardiff, CF24 4HQ, Wales, UK. Phone: +44 (0)29 20875064.
E-mail: QuantockAJ@cardiff.ac.uk

Submitted: 24 April, 2020. *Accepted:* 11 May, 2020.

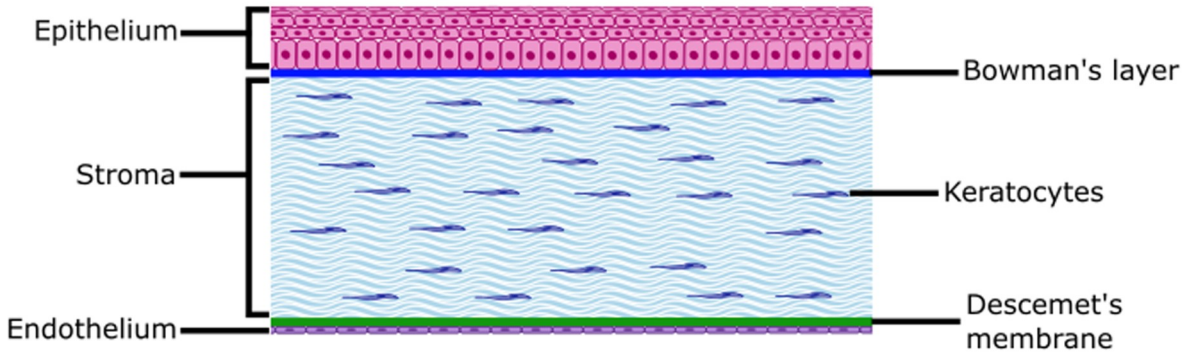

Fig 1. Corneal structure. Depending on the species, the cornea consists of four or five layers. From anterior to posterior, the cellular layers comprise the epithelium, stroma, and endothelium. Descemet's membrane is the basement membrane of the endothelium and, where present, Bowman's layer is an acellular condensation of collagen.

endothelium itself, which is a monolayer of metabolically active cells separating the cornea from the aqueous environment of the inner eye.

Interestingly, not all species appear to possess a Bowman's layer. An electron microscopic study by Hayashi and colleagues (2002) suggests that in those that do its thickness ranges from approximately 1 µm (rat) to 10 µm (human). Likewise, Komai and Ushiki (1991) and Morishige and associates (2006) report that in humans Bowman's layer is 8-12 µm thick. It consists mostly of collagen types I, III, V and VI (Marshall et al. 1991b, a), with the diameter of the collagen fibrils in the range of 20-36 nm (Kayes and Holmberg 1960; Teng 1962).

The function of Bowman's layer is debated, particularly as it is not present in all animals. It has been suggested that this dense, interwoven meshwork of collagen fibrils beneath the surface of the cornea might play a biomechanical role, helping to maintain the cornea's proper curvature. Indeed, breaks in Bowman's membrane have been reported in a condition called keratoconus (Sawaguchi et al., 1998), a disease of unknown cause in which a patient's cornea becomes progressively thinner and more "cone-like". However, the observation that photorefractive keratectomy, an ablative laser surgery that reshapes the front surface of the cornea and which removes Bowman's layer, does not cause corneal ectasia (Wilson and Hong, 2000) could mean Bowman's layer may be less important for maintaining the corneal curvature (and thus the eye's refractive status). It has also been suggested that the acellularity of Bowman's layer imparts a protective function by preventing the spread of infections from the epithelium to the stroma (Wilson and Hong, 2000).

Whether or not there is a Bowman's layer in the porcine cornea is currently contested. Several sources mention observing Bowman's layer (Bueno et al., 2011; Du et al., 2011; Zhang et al., 2019), but there have been reports claiming its absence in porcine tissue (Merindano et al., 2002; Svaldenienė et al., 2003; Nautscher et al., 2016; Patruno et al., 2017). Here, we show that Bowman's layer is indeed a feature of the porcine cornea, and reveal that an abrupt and significant increase in the non-random alignment of collagen fibrils in Bowman's layer occurs at the periphery of the cornea, where it merges with the sclera of the eye, just before its termination.

MATERIALS AND METHODS

Tissue acquisition

Four porcine eyes, sourced from a local abattoir (W.T. Maddock, Kembery Meats, Maesteg, Wales, UK), were dissected within hours of slaughter. First, corneoscleral discs were manually dissected from whole eye globes. Four limbal tissue segments of approximately 2 mm x 4 mm were dissected from three of the corneas. These segments

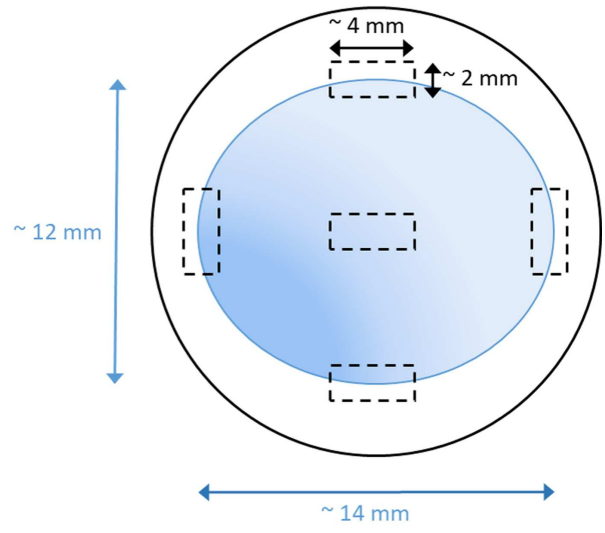

Fig 2. Tissue segments were taken from four limbal sites in the porcine cornea after identification of the horizontal and vertical meridians from measurements of corneal diameters. The central cornea was also sampled. White area = sclera, blue area = cornea. Not to scale.

comprise scleral and peripheral corneal tissue and were taken from the assumed 3, 6, 9 and 12 o'clock positions (Fig. 2) after corneas had been oriented by measuring the longest and shortest diameters of the oval-shaped corneas, and assuming the longest diameter to be the horizontal meridian (Sanchez et al., 2011). Similarly sized central corneal segments were also dissected from the same corneas. The remaining cornea had a central corneal segment and one limbal segment dissected. The samples from the first three corneas were then prepared for scanning electron microscopy (SEM) and the central and limbal segments from the remaining cornea were prepared for transmission electron microscopy (TEM).

Transmission electron microscopy

The central corneal segment and limbal segment for TEM were immediately fixed in 2.5% glutaraldehyde/2% paraformaldehyde (PFA) in 0.1 M sodium cacodylate buffer (pH 7.2) overnight at 4°C. The segments were then washed in 0.1 M sodium cacodylate buffer and processed using a modification of the method described by Deerinck et al. (2010) that provides high contrast for observation of general cell and tissue morphology. All solutions and distilled water were passed through Minisart® syringe filters (Sartorius Stedim Biotech GmbH, Goettingen, Germany) onto the tissue sample. Next, the tissue was immersed in 1.5% potassium ferricyanide/1% osmium tetroxide for 1 hour, followed by washing in distilled water. The samples were then transferred to 1% aqueous thiocarbohydrazide for 30 mins, again followed by washing in distilled water. After this, the samples were immersed in 1% osmium tetroxide followed by 1% aqueous uranyl acetate, both for 1 hour each followed by a distilled water wash after each step. All of these steps were carried out at room temperature. The tissue was then immersed in Walton's lead aspartate for 1 hour at 60°C. A distilled water wash was then carried out at room temperature once again. Next, the tissue was dehydrated in an ethanol series: first 70% then 90% (both for 15 mins), followed by 100% (2 x 15 mins) and then propylene oxide (2 x 15 mins). The tissue was then placed in a 1:1 mixture of Araldite CY212 epoxy resin, without benzyl dimethylamine (BDMA) accelerator, and propylene oxide overnight. After several changes of Araldite resin without BDMA accelerator, the specimens received several changes of Araldite resin including the BDMA accelerator over two days. The segments were then placed into embedding moulds with further resin and polymerised in an oven at 60˚C for at least 24 hours.

Tissue sections of the polymerised blocks were cut using a Reichert-Jung Ultracut E microtome. The tissue segment was oriented inside the resin block so that radial sections were taken. Semi-thin sections of 300 nm thickness were cut first and stained with toluidine blue for light microscopy to select appropriate regions of interest. Ultrathin sections 100 nm thick were then cut using a diamond knife and collected on uncoated G300 copper electron microscopy grids (Gilder Grids, Grantham, UK). The sections were imaged using a Jeol 1010 transmission electron microscope (Jeol (UK) Ltd, Welwyn Garden City, UK) in Cardiff University. Unless specified, all reagents and equipment are from Agar Scientific Ltd (Stansted, UK) or Taab Laboratory Equipment Ltd (Aldermaston, UK).

Scanning electron microscopy

All tissue segments from the other three corneas were fixed in 2.5% glutaraldehyde/2% PFA in 0.1 M sodium cacodylate buffer (pH 7.2) for approximately 16 hours at room temperature. They were then washed in 0.1 M sodium cacodylate buffer. Cell maceration was carried out by immersing the tissue segments in 10% aqueous sodium hydroxide over five days at room temperature. They were then washed in distilled water over approximately 24 hours. The samples were then transferred to aqueous 2% tannic acid for 6 hours. The tissue segments were washed in distilled water again, followed by immersion in aqueous 1% osmium tetroxide for 2 hours. After another wash in distilled water, the tissue segments were dehydrated in an ethanol series, going from 70% to 90% (both 1 x 30 mins) to 100% (2 x 30 mins). The tissue was then dried using hexamethyl-disilazane (HMDS) (Thermo Fisher Scientific, Heysham, UK). The tissue segments were transferred to a 1:1 solution of 100% ethanol and HMDS for 1 hour, followed by 2 x 1 hour in 100% HMDS. The tissue segments were then left in fresh HMDS in a desiccator in a fume hood until all of the liquid had evaporated. Finally, the dehydrated tissue segments were mounted on 12.5 mm aluminium stubs and then coated with ~15 nm gold-palladium, using a Biorad SC500 sputter coater with argon as the sputtering gas. In- lens secondary electron images were acquired on a Zeiss Sigma HD field emission gun scanning electron microscope (Carl Zeiss Ltd, Cambridge, UK) in Cardiff University under high vacuum conditions. A beam energy of 5 kV was used with a 30 µm final aperture and a nominal beam current of ~150 pA. Working distance was maintained at approximately 5 mm and images were acquired at 5,000, 10,000 and 50,000x magnification. Again, unless specified, all reagents and equipment are from Agar Scientific Ltd (Stansted, UK) or Taab Laboratory Equipment Ltd (Aldermaston, UK).

The orientation of the ocular surface collagen fibrils was assessed using the ImageJ/Fiji plug-in "FibrilTool" (Boudaoud et al., 2014). Three distinct areas in each limbal sample were identified for quantification of fibril alignment: peripheral cornea, a transition zone and the limbal annulus of collagen. The images used for quantification were ac-

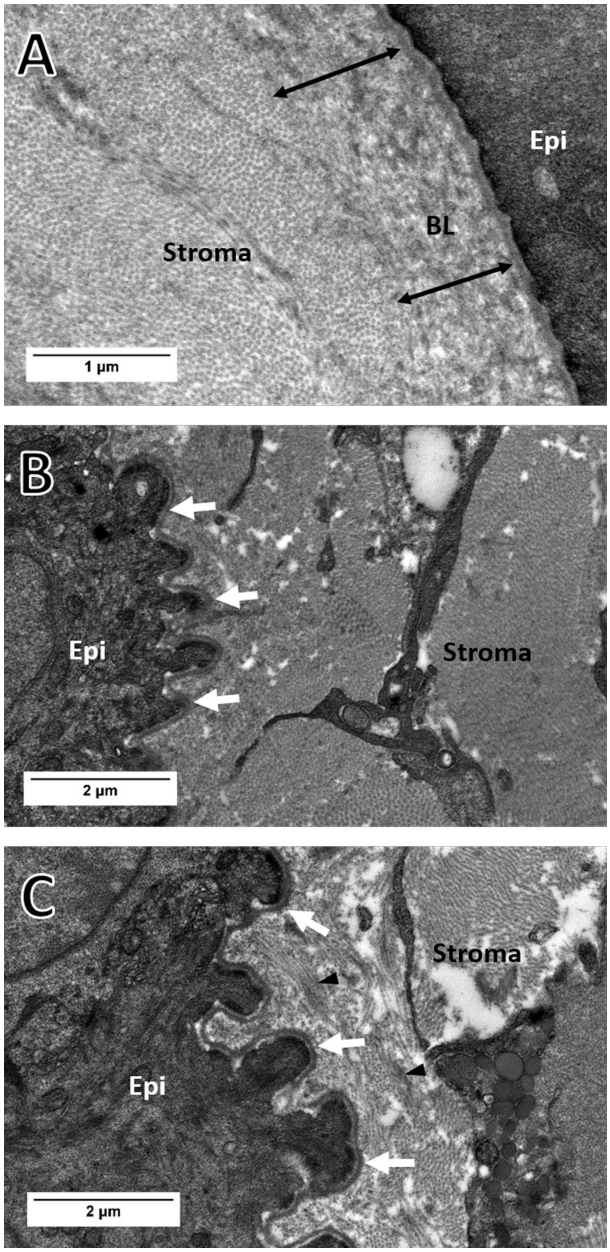

Fig 3. Transmission electron micrographs of the superficial porcine corneal and limbal stroma. **A**: a band of disorganised collagen fibrils beneath the epithelial basement membrane in the central cornea that is consistent with the anatomical appearance of Bowman's layer (black arrows). **B, C**: the basement membrane at the limbus exhibits an irregular profile (white arrows) compared to central cornea and the collagen fibrils immediately subjacent to it appear more organised than those in the putative Bowman's layer. Most of the fibrils can be seen in transverse section, suggesting this is the annulus of collagen around the limbal circumference, with some fibril bundles visible also (C, black arrowheads). Epi = epithelium, BL = Bowman's layer.

quired at 10,000x magnification; one from each of the three areas in all four limbal sites from the three eyes, and four from the central cornea of each eye. FibrilTool was applied to the same five set regions of interest in each image examined, resulting in 60 values generated for each distinct area (central cornea, peripheral cornea, transition zone and limbal annulus) across three eyes.

The means were calculated from these values and independent samples Student's T-test was then performed to compare the averages.

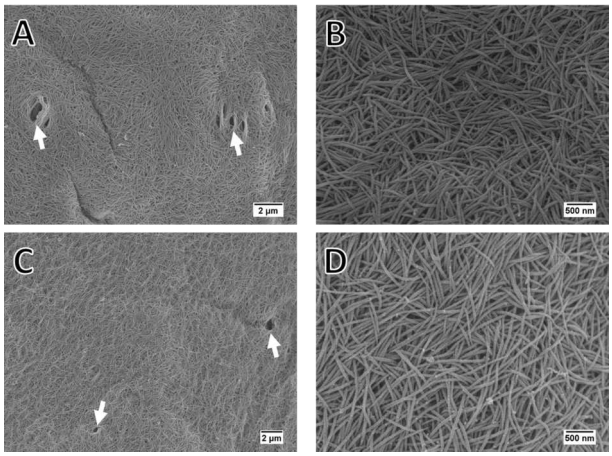

Fig 4. Scanning electron micrographs of the decellularised central corneal surface (**A, B**) and the peripheral corneal surface (**C, D**). Collagen fibrils demonstrate no alignment but rather a completely random distribution with much interweaving. Occasional pores can be seen in both the central and peripheral corneal surface (arrows).

RESULTS

Transmission electron microscopy

Subjacent to the epithelial basement membrane of the central cornea, a band of unorganised collagen fibrils was found lying distally to typical lamellae of the central cornea characterised by collagen fibrils with highly regular orientation (Fig. 3A). This unorganised band of fibrils varied in thickness between approximately 1-2 µm, and was not detected in images of the porcine limbus (Fig. 3B, C). In the limbus, the epithelial basement membrane profile appeared less regular than at the corneal centre together with a predominance of transversely-sectioned collagen fibrils, consistent with the appearance of the limbal annulus of collagen.

Scanning electron microscopy

Observations of the decellularised anterior surface of the central cornea revealed no apparent organisation or alignment of the collagen fibrils (Fig. 4A, B). Instead, an interweaving mesh of uniform diameter collagen fibrils was observed. The peripheral corneal surface has the same appearance as the central cornea (Fig. 4C, D). Pores of varying sizes occur sporadically within the ocular surface across both the central and peripheral cornea.

The limbal region can be separated into three distinct areas (Fig. 5): the peripheral cornea as mentioned above, a "transition zone" and the limbal annulus of collagen. The sclera can also be seen beyond the limbal annulus. These areas are distinguished by the variation in alignment of their collagen fibrils.

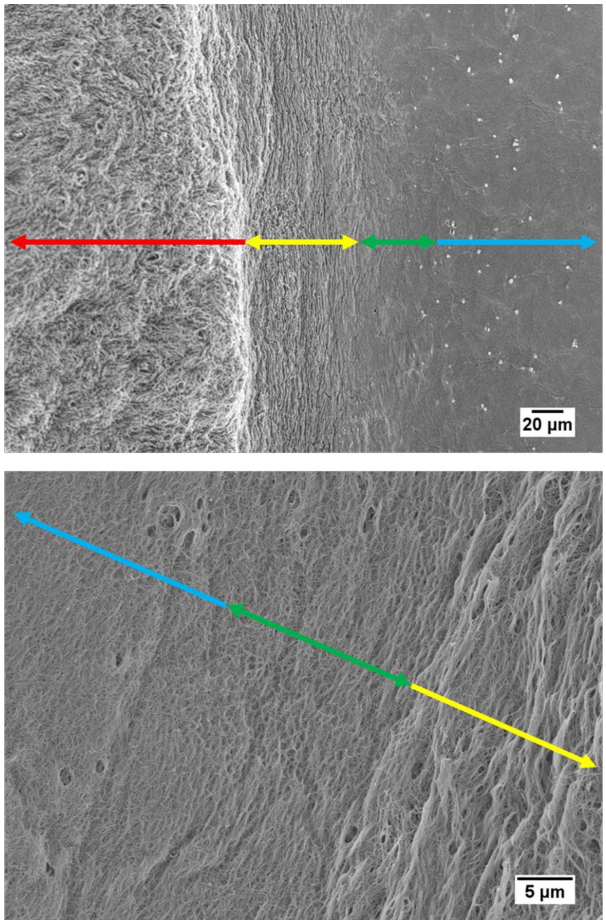

Fig 5. Scanning electron micrographs across the decellularised limbal surface demonstrating the different zones of the limbus. The peripheral cornea (blue arrow) and limbal annulus (yellow arrow) are separated by a transition zone (green arrow) where collagen fibrils start to become more aligned. Collagen architecture shows a noticeable change moving from the limbus to the sclera (red arrow).

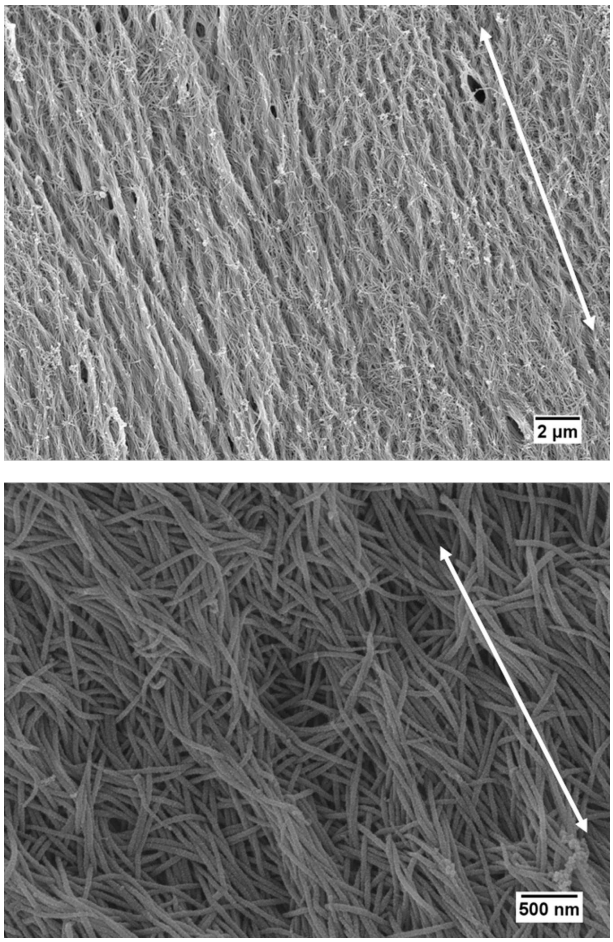

Fig 6. Scanning electron micrographs of the decellularised corneolimbal surface. A transition zone exists between the presumed Bowman's layer and the limbal annulus of collagen, where the collagen fibrils start to align more than in the central or peripheral cornea. Interweaving of fibrils persists and the level of alignment is noticeably less than in the limbal annulus. White arrows represent the direction of alignment as determined by FibrilTool.

The transition zone represents an area where the change from disorganised peripheral cornea to the highly aligned limbal annulus could be seen (Fig. 5, green arrow and Fig. 6). In this area, collagen fibrils exhibit greater alignment than in the peripheral cornea, but cross-cutting, interweaving fibrils are still evident.

Beyond the transition zone, a band of highly aligned collagen fibrils was seen (Fig. 5, yellow arrow and Fig. 7). We believe this represents the limbal annulus of collagen where fibrils run circumferentially around the cornea, which has been identified previously in human and porcine eyes (Newton and Meek, 1998; Meek and Boote, 2004; Hayes et al., 2007). The collagen fibrils here almost all align, and often group into bundles, forming ridges. The direction of alignment was parallel to the limbal circumference.

The change in fibril alignment from the limbus to scleral surface was very noticeable, both at lower (Fig. 5, red arrow) and higher magnifications. The change was, however, much more evident at higher magnification as the reduction in collagen fibril organisation can be more clearly seen (Fig. 8). Though the fibrils were once again unaligned, the appearance of the sclera differed greatly from the central and peripheral cornea. Collagen fibrils arranged in bundles give rise to many pores across the scleral surface, in contrast to the very flat surface of unaligned fibrils observed in the central and peripheral cornea.

Quantification of collagen fibril alignment

Using the FibrilTool plug-in for ImageJ, the alignment of fibrils can be quantified. This software measures the anisotropy of fibre arrays within an image and produces a value between 0 (no alignment) and 1 (perfectly aligned) (Boudaoud et al., 2014).

The central and peripheral cornea both generate low, but different, values for alignment of their collagen fibrils (0.08 ± 0.04 and 0.11 ± 0.05 respectively). Interestingly, this difference was found to be

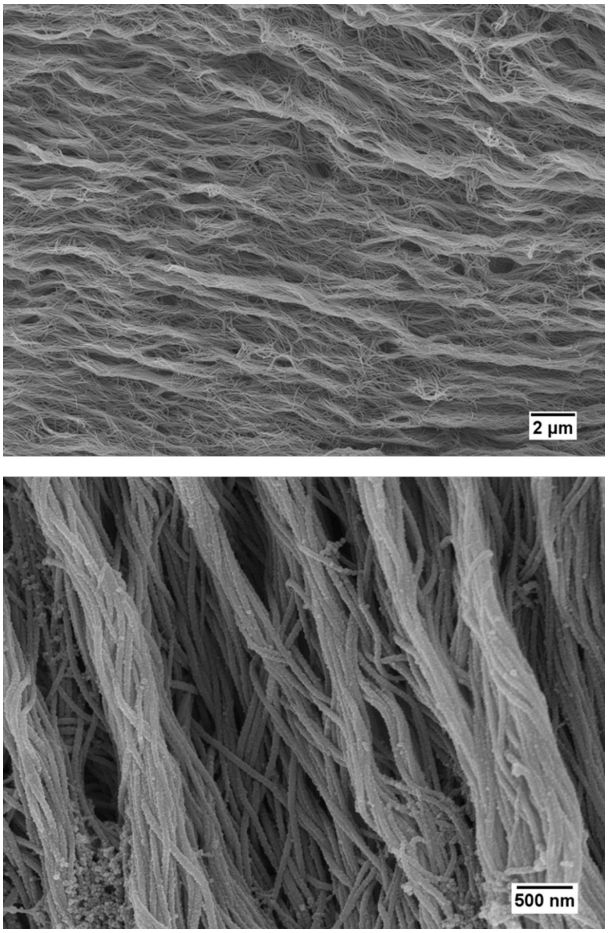

Fig 7. Scanning electron micrographs of the decellularised limbus, revealing the limbal annulus of collagen. Collagen fibrils show a much greater degree of alignment here than elsewhere. The direction of alignment is parallel to the limbal circumference.

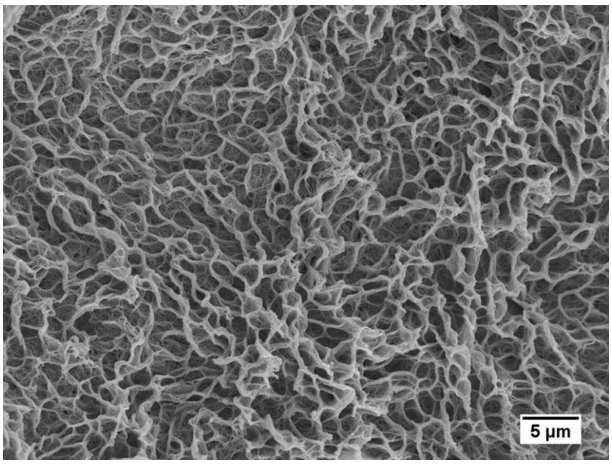

Fig 8. Scanning electron micrograph of the decellularised scleral surface. Here collagen fibrils associate in bundles but there is no alignment between respective bundles, creating a very irregular and disorganised surface profile. The morphology is very different to that of the cornea and limbus.

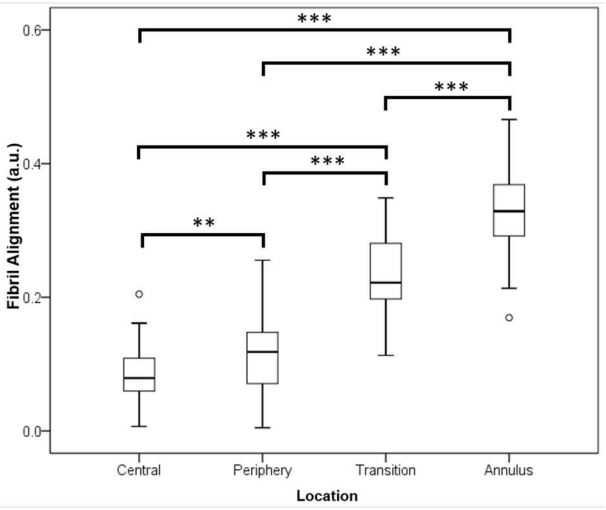

Fig 9. Collagen fibril alignment, as determined by FibrilTool, increases significantly with increasing corneal eccentricity. The central corneal surface has the lowest level of anisotropy, with statistically significant increases in all the areas found in the corneolimbal region. Despite the significant increase in fibril alignment between the central and peripheral corneal stromal surfaces, the low anisotropy values for these areas is taken to be confirmatory of the existence of Bowman's layer in the porcine cornea. ** $p < 0.01$, *** $p < 0.001$.

statistically significant ($p < 0.01$). There was a much larger increase in the alignment of collagen fibrils in the transition zone with a value of 0.23 ± 0.06. This was significantly different to the central cornea and peripheral cornea (both $p < 0.001$). The collagen fibril alignment increased further in the limbal annulus to 0.33 ± 0.07, which was once again significantly different to all other regions ($p < 0.001$). These data are summarized in Fig. 9.

DISCUSSION

The presence of Bowman's layer within the porcine cornea has been disputed for a number of years, with several contradictory reports in the scientific literature (Merindano et al., 2002; Bueno et al., 2011; Du et al., 2011; Nautscher et al., 2016). However, in this investigation, we present images of porcine tissue that appear directly comparable to images of the human Bowman's layer produced by Birk (2001) and Hayashi et al. (2002). We also demonstrate a quantifiable change in the alignment of the collagen fibrils from the central cornea surface to the periphery and the limbus.

Using the measured thicknesses of Bowman's layer and of the substantia propria (stroma + Bowman's layer) from SEM and TEM images analysed by Hayashi and associates (2002), the relative percentage contribution of Bowman's layer to corneal thickness can be calculated (Table 1). This varies considerably between species, with those classically considered as lacking Bowman's layer often yielding a very low percentage. Based on an average thickness of 0.94 ± 0.15 µm for a potential porcine Bowman's layer (from measurements taken from 3 points across 10 images from this investigation using ImageJ), and an approximate stromal thickness between 465 and 573 µm, the

Table 1. The proportions of the substantia propria thickness, comprising stroma and Bowman's layer, that is contributed by Bowman's layer*. * Measurements for all species, except the pig, are from Hayashi et al. (2002).

Species	Thickness of Bowman's layer (µm)	Thickness of stroma + Bowman's layer (µm)	% of substantia propria thickness comprised of Bowman's layer
Rabbit	3	250	1.2
Guinea pig	1	270	0.4
Rat	1	88	1.1
Pig	0.94	~465-573	0.2
Cow	5	800	0.6
Human	10	340	2.9

porcine Bowman's layer would comprise approximately 0.2% of corneal thickness. The stromal thickness measurements are based on central corneal thickness measurements of ex vivo porcine eyes obtained from the same source as the current investigation by Akhbanbetova et al. (2017) and porcine epithelial thickness measurements by Nautscher et al. (2016) and Abhari et al. (2018). This very low representative proportion of total corneal thickness may explain why the Bowman's layer in this species has sometimes been overlooked. A lack of imaging resolution may have prevented identification of this structure in previous investigations.

In all species examined by Hayashi and associates, the epithelial surface of Bowman's layer demonstrates a mesh of randomly arranged collagen fibrils, in contrast to the highly-aligned, parallel collagen fibrils of the corneal stromal lamellae. The appearance of the human Bowman's layer is similar to that described in Komai and Ushiki's investigation (1991). Our investigation shows that the decellularised epithelial surface of central porcine cornea demonstrates the same disorganised collagen fibril arrangement. Differences in the appearance of the epithelial surface of Bowman's layer exist between species. The porcine Bowman's layer is most similar to the rat and rabbit corneas presented in Hayashi et al.'s report and to the human Bowman's layer in Komai and Ushiki's investigation. This includes the presence of multiple pores across the surface of Bowman's layer that, Komai and Ushiki presumed, are channels for nerve fibres to reach the corneal epithelium.

The peripheral cornea of the porcine eye demonstrates the same organisation as the central cornea, implying that there is a structure representative of Bowman's layer in the porcine cornea. This includes the presence of pores, which may be the conduits for corneal innervation. However, these pores could also represent a route for the passage of processes from stromal cells that extend towards, and make direct contact with, the basal epithelium. These keratocyte processes have been identified, and their direct interaction with epithelial cells confirmed, in the peripheral cornea/limbal region of rabbits and humans (Dziasko et al., 2014; Yamada et al., 2015).

The limbal collagen fibrils of the porcine cornea are arranged in a significantly different manner than those of the central and peripheral cornea. This was predicted due to Bowman's layer terminating at the limbus. We have identified a "transition zone" between the disorganised peripheral Bowman's layer and the highly aligned limbal annulus of collagen. Here, collagen fibrils exhibit initial stages of alignment, though there is still a significant degree of isotropy. The statistically significant differences in fibril alignments between the transition zone and the peripheral Bowman's layer, and between the transition zone and the limbal annulus, further demonstrate the distinct nature of this zone.

An interesting and unexpected finding is the significant increase in collagen fibril alignment from the central Bowman's layer to the periphery. Visually, the two regions look identical, but quantification of collagen fibril anisotropy confirms this increase in organisation. Potentially, this could mean that the fibrils of Bowman's layer do very gradually become more aligned with increasing corneal eccentricity, before a sudden increase in alignment in the transition zone, which marks the termination of this layer. This requires further investigation, examining the entire corneal surface.

In conclusion, from observations and from measurements of the organisation of collagen fibrils in scanning electron microscopy images, it appears that the porcine cornea does include a Bowman's layer. Quantification of collagen fibril alignment further supports this by clearly demonstrating the unorganised nature of the central/peripheral decellularised corneal surface collagen fibrils and the significant increase in fibril alignment in the limbal annulus of collagen and the newly identified, intermediate transition zone. This shows the porcine cornea's similarity to its human counterpart and further supports its use as a model for the human cornea.

ACKNOWLEDGEMENTS

This work was supported by the Biotechnology and Biological Sciences Research Council-funded South West Biosciences Doctoral Training Partnership, Grant reference BB/M009122/1.

REFERENCES

ABHARI S, EISENBACK M, KAPLAN HJ, W ALTERS E, PRATHER RS, SCOTT PA (2018) Anatomic studies of the miniature swine cornea. Anat Rec, 301: 1955-1967.

AKHBANBETOVA A, NAKANO S, LITTLECHILD SL, YOUNG RD, ZVIRGZDINA M, FULLWOOD NJ, WESTON I, WESTON P, KINOSHITA S, OKUMURA N, KOIZUMI N, QUANTOCK AJ (2017) A surgical cryoprobe for targeted transcorneal freezing and endothelial cell removal. J Ophthalmol, 2017: 5614089.

BIRK DE (2001) Type V collagen: Heterotypic type I/V collagen interactions in the regulation of fibril assembly. Micron, 32: 223-237.

BOUDAOUD A, BURIAN A, BOROW SKA-W YKRĘT D, UYTTEWAAL M, WRZALIK R, KWIATKOWSKA D, HAMANT O (2014) FibrilTool, an ImageJ plug-in to quantify fibrillar structures in raw microscopy images. Nat Protoc, 9: 457-463.

BUENO JM, GUALDA EJ, ARTAL P (2011) Analysis of corneal stroma organization with wave front optimized nonlinear microscopy. Cornea, 30: 692-701.

DEERINCK TJ, BUSHONG EA, THOR A, ELLISMAN MH (2010) NCMIR methods for 3D EM: A new protocol for preparation of biological specimens for serial block face scanning electron microscopy [Online]. Available at: http://ncmir.ucsd.edu/sbfsem-protocol.pdf. [Accessed: 20/08/2019].

DU L, WU X, PANG K, YANG Y (2011) Histological evaluation and biomechanical characterisation of an acellular porcine cornea scaffold. Br J Ophthalmol, 95: 410-414.

DZIASKO MA, ARMER HE, LEVIS HJ, SHORTT AJ, TUFT S, DANIELS JT (2014) Localisation of epithelial cells capable of holoclone formation in vitro and direct interaction with stromal cells in the native human limbal crypt. PLoS One, 9: e94283.

HAYASHI S, OSAWA T, TOHYAMA K (2002) Comparative observations on corneas, with special reference to Bowman's layer and Descemet's membrane in mammals and amphibians. J Morphol, 254: 247-258.

HAYES S, BOOTE C, LEW IS J, SHEPPARD J, ABAHUSSIN M, QUANTOCK AJ, PURSLOW C, VOTRUBA M, MEEK KM (2007) Comparative study of fibrillar collagen arrangement in the corneas of primates and other mammals. Anat Rec, 290: 1542-1550.

KAYES J, HOLMBERG A (1960) The fine structure of Bowman's layer and the basement membrane of the corneal epithelium. Am J Ophthalmol, 50: 1013-1021.

KOMAI Y, USHIKI T (1991) The three-dimensional organization of collagen fibrils in the human cornea and sclera. Invest Ophthalmol Vis Sci, 32: 2244-2258.

MARSHALL GE, KONSTAS AG, LEE WR (1991a) Immunogold fine structural localization of extracellular matrix components in aged human cornea II. Collagen types V and VI. Graefes Arch Clin Exp Ophthalmol, 229: 164-171.

MARSHALL GE, KONSTAS AG, LEE WR (1991b) Immunogold fine structural localization of extracellular matrix components in aged human cornea. I. Collagen types I-IV and laminin. Graefes Arch Clin Exp Ophthalmol, 229: 157-163.

MEEK KM, BOOTE C (2004) The organization of collagen in the corneal stroma. Exp Eye Res, 78: 503-512.

MERINDANO MD, COSTA J, CANALS M, POTAU JM, RUANO D (2002) A comparative study of Bowman's layer in some mammals: Relationships with other constituent corneal structures. Eur J Anat, 6: 133-139.

MORISHIGE N, PETROLL WM, NISHIDA T, KENNEY MC, JESTER JV (2006) Noninvasive corneal stromal collagen imaging using two-photon-generated second-harmonic signals. J Cataract Refract Surg, 32: 1784-1791.

NAUTSCHER N, BAUER A, STEFFL M, AMSELGRUBER WM (2016) Comparative morphological evaluation of domestic animal cornea. Vet Ophthalmol, 19: 297-304.

NEWTON RH, MEEK KM (1998) Circumcorneal annulus of collagen fibrils in the human limbus. Invest Ophthalmol Vis Sci, 39: 1125-1134.

PATRUNO M, PERAZZI A, MARTINELLO T, BLASEOTTO A, DI IORIO E, IACOPETTI I (2017) Morphological description of limbal epithelium: searching for stem cells crypts in the dog, cat, pig, cow, sheep and horse. Vet Res Commun, 41: 169-173.

SANCHEZ I, MARTIN R, USSA F, FERNANDEZ-BUENO I (2011) The parameters of the porcine eyeball. Graefes Arch Clin Exp Ophthalmol, 249: 475-482.

SAW AGUCHI S, FUKUCHI T, ABE H, KAIYA T, SUGAR J, YUE BYJT (1998) Three-dimensional scanning electron microscopic study of keratoconus corneas. Arch Ophthalmol, 116: 62-68.

SVALDENIENĖ E, BABAUSKIENĖ V, PAUNKSNIENĖ M (2003) Structural features of the cornea: Light and electron microscopy. Vet Zootec, 24: 50-55.

TENG CC (1962) Fine structure of the human cornea: Epithelium and stroma. Am J Ophthalmol, 54: 969-1002.

WILSON SE, HONG J (2000) Bowman's layer structure and function: Critical or dispensable to corneal function? A hypothesis. Cornea, 19: 417-420.

YAMADA K, YOUNG RD, LEWIS PN, SHINOMIYA K, MEEK KM, KINOSHITA S, CATERSON B, QUANTOCK AJ (2015) Mesenchymal–epithelial cell interactions and proteoglycan matrix composition in the presumptive stem cell niche of the rabbit corneal limbus. Mol Vis, 21: 1328-1339.

ZHANG K, REN X-X, LI P, PANG K-P, W ANG H (2019) Construction of a full-thickness human corneal substitute from anterior acellular porcine corneal matrix and human corneal cells. Int J Ophthalmol, 12: 351-362.